Anthropogenic climate change drives non-stationary phytoplankton variance

Geneviève W. Elsworth[1], Nicole S. Lovenduski[2], Kristen M. Krumhardt[3], Thomas M. Marchitto[1], and Sarah Schlunegger[4]

[1]Department of Geological Sciences and Institute of Arctic and Alpine Research, University of Colorado Boulder, Boulder, Colorado, USA
[2]Department of Atmospheric and Oceanic Sciences and Institute of Arctic and Alpine Research, University of Colorado Boulder, Boulder, Colorado, USA
[3]Climate and Global Dynamics Laboratory, National Center for Atmospheric Research, Boulder, Colorado, USA
[4]Department of Atmospheric and Oceanic Sciences, Princeton University, Princeton, New Jersey, USA

Correspondence to: Geneviève Elsworth (genevieve.elsworth@colorado.edu)

Abstract. Multiple studies conducted with Earth System Models suggest that anthropogenic climate change will influence marine phytoplankton over the coming century. Light limited regions are projected to become more productive and nutrient limited regions less productive. Anthropogenic climate change can influence not only the mean state, but also the variance around the mean state, yet little is known about how variance in marine phytoplankton will change with time. Here, we quantify the influence of anthropogenic climate change on internal variability in marine phytoplankton biomass from 1920 to 2100 using the Community Earth System Model 1 Large Ensemble (CESM1-LE). We find a significant decrease in the internal variance of global phytoplankton carbon biomass under a high emission (RCP8.5) scenario, with heterogeneous regional trends. Decreasing variance in biomass is most apparent in the subpolar North Atlantic and North Pacific. In these high-latitude regions, ~~zooplankton grazing acts as a top-down control in reducing internal variance in phytoplankton biomass, with~~ bottom-up controls (e.g., light, nutrients) ~~having~~ have only a small effect on biomass variance. ~~Grazing-driven declines in phytoplankton variance are also apparent~~ Rather, the declining internal variability co-occurs with a reduction in zooplankton grazing variability. Similar patterns emerge in the biogeochemically critical regions of the Southern Ocean and the Equatorial Pacific. Our results suggest that climate mitigation and adaptation efforts that account for marine phytoplankton changes (e.g., fisheries) should also consider changes in phytoplankton and zooplankton variance driven by anthropogenic warming, particularly on regional scales.

1 Introduction

Anthropogenic climate change has significantly impacted marine ecosystems from phytoplankton (Bopp et al., 2001, 2013; Laufkötter et al., 2015; Kwiatkowski et al., 2020) to fish (Perry et al., 2005; Cheung et al., 2009, 2010; Mills et al., 2013; Wernberg et al., 2016; Flanagan et al., 2018; Staudinger et al., 2019). As the base of the marine food web, phytoplankton support diverse marine ecosystems by providing food for higher trophic levels (Falkowski, 2012). Constraining future changes in phytoplankton with anthropogenic warming is important at regional scales for fisheries adaptation (Pauly and Christensen,

1995; Chassot et al., 2010; Link and Marshak, 2019; Marshak and Link, 2021), particularly as phytoplankton biomass is incorporated into offline fisheries models to predict changing catch potential (Christensen and Walters, 2004; Travers-Trolet et al., 2009; Lehodey et al., 2010; Maury, 2010; Blanchard et al., 2012; Christensen et al., 2015; Jennings and Collingridge, 2015; Tittensor et al., 2018; Petrik et al., 2019; Heneghan et al., 2021). In this context, understanding changes in both phytoplankton biomass and its variance is essential in reducing uncertainty in marine ecosystem projections.

The abundance and distribution of phytoplankton, the base of the marine food web, will likely change with anthropogenic warming. Future projections of climate change impacts reveal a global loss of marine net primary production (NPP) and phytoplankton biomass, particularly at middle and low latitudes (Steinacher et al., 2010; Bopp et al., 2013; Lotze et al., 2019; Tittensor et al., 2021). A majority of Earth System Models (ESMs) project an increase in phytoplankton abundance in the high latitude ocean as light limitation is alleviated by stratification, increasing temperature stimulates photosynthesis, and sea ice cover declines (Steinacher et al., 2010; Bopp et al., 2013). In contrast, a decrease in the low latitude oceans is projected as nutrient limitation from thermal stratification is enhanced (Steinacher et al., 2010; Kwiatkowski et al., 2020). While bottom-up controls (e.g., nutrient flux, light availability) have been shown to affect phytoplankton growth in a changing climate, top-down controls (i.e., zooplankton grazing) also play a role. For example, analysis across a suite of models forced under climate change scenarios revealed grazing pressure as a driver of biomass decline in low to intermediate latitude regions (Laufkötter et al., 2015). Additionally, top-down controls have been shown to affect regional changes in NPP and export production (Bopp et al., 2001), as well as the timing of phytoplankton bloom onset (Yamaguchi et al., 2022). Regional redistributions of phytoplankton biomass have consequences for fisheries management and conservation (Blanchard et al., 2017; Stock et al., 2017), and may have implications for economics and policy making decisions (Moore et al., 2021).

While climate change is known to impact the mean state of phytoplankton biomass or NPP (Bopp et al., 2013; Kwiatkowski et al., 2020), less is known about how climate change will affect variability in these quantities. One recent modeling study found that ~~the~~ climate change alters the timing of seasonal blooms in many regions of the global ocean, an effect that could be realized by the end of the century (Yamaguchi et al., 2022) Several other recent studies have demonstrated how other aspects of the coupled atmosphere-ocean climate system are projected to experience changes in variance in a changing climate (Resplandy et al., 2015; Landschützer et al., 2018; Kwiatkowski and Orr, 2018; Rodgers et al., 2021). For example, Resplandy et al. (2015) examined the contribution of internal variability to air-sea pCO_2 and pO_2 fluxes with climate change using a suite of ESMs. Their analyses revealed distinct regional differences in variability of air-sea pCO_2 and pO_2 fluxes. Other studies have revealed increases in the frequency of modes of internal variability such as El Niño and La Niña events in response to greenhouse warming (Timmermann et al., 1999; Cai et al., 2014, 2015, 2022). Clarifying how variance in phytoplankton biomass may be changing over long time scales with climate change is important for fisheries management, especially at regional scales, as it affects our ability to make accurate near-term predictions of fisheries production. Near-term predictions of phytoplankton biomass may also benefit from knowledge of the projected magnitude of internal variability, as the chaotic nature of internal variability hampers near-term predictions (Meehl et al., 2009, 2014). However, modeled internal variability may differ from that observed in the real world.

Here, we quantify changes in the internal variability (ensemble spread) of phytoplankton biomass over the next century using a large ensemble of an ESM, in which each ensemble member experiences a different phasing of internal climate variability but is forced with a common emissions scenario. We illustrate the drivers of these changes in variance via statistical analysis of physical and biogeochemical model output and demonstrate their relative importance in key fisheries regions. While we recognize that an ESM (and indeed, the real world) is a complex, nonlinear system, we approximate at first-order the linear relationships between key variables to attribute drivers of change in phytoplankton biomass variance.

2 Methods

2.1 Community Earth System Model 1 Large Ensemble

2.1.1 Model Description

We evaluate changes in phytoplankton biomass variance using output from the Community Earth System Model 1 Large Ensemble (CESM1-LE) (Kay et al., 2015). CESM1 is a fully-coupled climate model that simulates Earth's climate under historical and Representative Concentration Pathway (RCP) 8.5 external forcing by simulating the evolution of coupled atmosphere, ocean, land, and sea ice component models (Hurrell et al., 2013). The ocean physical model is the ocean component of the Community Climate System Model version 4 (Danabasoglu et al., 2012) and has a nominal 1° resolution and 60 vertical levels. The Parallel Ocean Program version 2 (POP2) ocean model consists of an upper-ocean ecological module which incorporates multi-nutrient co-limitation of nitrate, ammonium, phosphate, dissolved iron, and silicate on phytoplankton growth and dynamic iron cycling (Moore et al., 2004; Doney et al., 2006; Moore and Braucher, 2008). The Biogeochemical Elemental Cycle (BEC) model simulates three phytoplankton functional types (PFTs): diatoms, diazotrophs, and small phytoplankton (i.e., cyanobacteria, nanophytoplankton, picoeukaryotes). Each PFT plays a unique role in the marine ecosystem and occupies a distinct ecological niche. For example, diatoms grow faster in cool, high-nutrient environments while small phytoplankton thrive in warmer, low-nutrient environments. In contrast, diazotrophs are not limited by nitrogen availability due to their ability to biologically fix nitrogen from the atmosphere. Each PFT has a maximum growth rate, which is dictated by temperature (scaled by a temperature function with a Q10 of 2.0), and limited by nutrient and light availability (Moore et al., 2004, 2013). Anthropogenic warming can alter these environmental variables and, in turn, affect phytoplankton abundance and productivity. Photoadaptation (variable chlorophyll to carbon ratios) occurs in response to variations in irradiance and nutrient availability (Geider et al., 1998; Moore et al., 2004). In addition to these bottom-up controls, top-down controls, such as zooplankton grazing, can also affect phytoplankton biomass. The ecosystem model simulates a single generic zooplankton functional type (ZFT) with different grazing rates and half saturation constants prescribed for different PFTs (e.g., slower zooplankton grazing rates for larger phytoplankton i.e., diatoms). Grazing rate is computed using a Holling Type III (sigmoidal) relationship and is a function of both prey density and temperature (Figure S1, Equation 5). Zooplankton loss is a function of a linear mortality term which represents natural mortality and a non-linear predation term which represents losses from predation. Both of

these loss terms scale with temperature. While zooplankton growth and loss terms both scale with temperature, a non-linear parameterization of the loss term results in a relatively larger increase in loss than increase in production with warming.

Large ensembles of ESMs are a recently developed research tool which allow us to disentangle fluctuations due to internal climate variability from those imposed by externally forced anthropogenic trends. Internal variability refers to variability in the climate system which occurs in the absence of external forcing, and includes processes related to the coupled ocean-atmosphere system (e.g., El Niño Southern Oscillation, Pacific Decadal Oscillation) (Santer et al., 2011; Deser et al., 2010; Meehl et al., 2013). In contrast, external forcing refers to the signal imposed by processes external to the climate system, such as solar variability, volcanic eruptions, and rising greenhouse gases from fossil fuel combustion (Deser et al., 2012, 2010; Schneider and Deser, 2018). The CESM1-LE simulates the evolution of the climate system with multiple ensemble members, each initiated with slightly different atmospheric temperature fields and branched from a multi-century 1850 control simulation with constant pre-industrial forcing (Lamarque et al., 2010; Danabasoglu et al., 2012). ~~Once the control simulation achieved equilibrium with the 1850 forcing, ensemble members were integrated~~ The CESM1-LE simulates the evolution of the climate system from 1920 to 2100 ~~using round-off level differences in the initial air temperature field (Kay et al., 2015), resulting in each ensemble member experiencing a different evolution~~ with multiple ensemble members, each expressing a different phasing of internal climate variability ~~(e. g., each member has different phasing of climate modes such as El Niño Southern Oscillation).~~ while responding to a shared external forcing prescription (Kay et al., 2015). Variable phasing of internal climate variability (e.g., ENSO) across ensemble members can influence phytoplankton biomass variability through the propagation of physical climate variability to biologically relevant environmental variables. ~~For example, an ensemble member with a positive phasing of ENSO may display decreased phytoplankton biomass in the Eastern Equatorial Pacific due to decreased upwelling nutrient flux.~~ RCP8.5 forcing was applied from 2006 to 2100 (Meinshausen et al., 2011) with well-mixed greenhouse gases and short-lived aerosols projected by four different Integrated Assessment Models (Lamarque et al., 2010). A total of 40 ensemble members were generated for the CESM1-LE experiment. Six CESM1-LE members had corrupted ocean biogeochemistry, therefore, we use the 34 CESM1-LE members with valid ocean biogeochemistry.

2.1.2 Statistical Analysis of Model Output

Analyses were conducted using annual mean output at 1° resolution from 1920 to 2100. Changes in CESM1 phytoplankton variance can be assessed via statistical analysis of chlorophyll concentration, net primary productivity (NPP), or phytoplankton carbon concentration (an indicator of total biomass). In our analysis we focus on biomass (phytoplankton carbon concentration) because it is an important predictor variable in offline fisheries models (Christensen and Walters, 2004; Travers-Trolet et al., 2009; Lehodey et al., 2010; Maury, 2010; Blanchard et al., 2012; Christensen et al., 2015; Jennings and Collingridge, 2015; Tittensor et al., 2018). Additionally, under climate change scenarios, phytoplankton biomass may be a more reliable indicator than NPP of climate change impacts (Bopp et al., 2021). Vertical integrals (top 150m) of biomass carbon concentration from each PFT were calculated and then summed to create maps of total phytoplankton biomass.

We classified the marine environment into 11 ecologically cohesive biomes as in Tagliabue et al. (2021) and Vichi et al. (2011) (Figure S2), which are a consolidation of the 38 ecological regions defined in Longhurst (2007). The provinces were aggregated

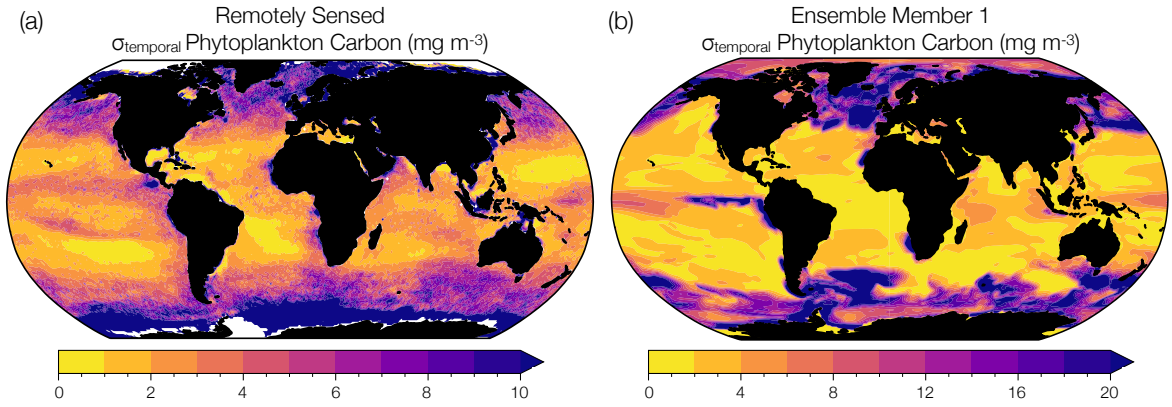

Figure 1. Comparison between observed and modeled phytoplankton biomass interannual variability. (a) Temporal standard deviation in annual mean phytoplankton carbon concentration (mg m^{-3}) reconstructed from remotely sensed chlorophyll concentrations, backscattering coefficients, and phytoplankton absorption (1998 to 2019) (Bellacicco et al., 2020). (b) Temporal standard deviation in annual mean phytoplankton carbon concentration (mg m^{-3}) simulated by ensemble member 1 of the CESM1-LE over the same observational period (1998 to 2019). Note the different magnitudes on the colorbars.

using multivariate statistical analysis ~~(Vichi et al., 2011).~~ of physical (i.e., salinity, temperature, mixed layer depth) and biological (i.e., chlorophyll concentration) ocean parameters to group ocean regions with similar physical and environmental conditions (Vichi et al., 2011). The ocean provinces were defined by randomly selecting from a combination of model and observational datasets and testing for statistical significance using analysis of similarities (ANOSIM) (Vichi et al., 2011). Although we consider all 11 biomes in our analysis, we analyze drivers in four biomes that are particularly relevant for fisheries production and/or of high biogeochemical interest: the subpolar Atlantic (ASP), the subarctic Pacific (SAP), the Equatorial Pacific (EQP), and the Southern Ocean (SOC) (Figure S2). ASP is a consolidation of aggregated biogeochemical provinces 4, 11, and 15, SAP a consolidation of 50 and 51, EQP a consolidation of 61, 62, and 63, and SOC a consolidation of 21, 81, 82, and 83 (Longhurst, 2007; Vichi et al., 2011) ~~.~~(Figure S2). Important biogeochemical regions are those characterized by coherent physical and environmental conditions, which support unique marine ecosystems and play an outsized role on global ocean biogeochemistry.

Internal variability at each location (x, y) is approximated as the standard deviation (σ) across ensemble members (EMs) at a given time (t),

$$\sigma(x, y, t) = \sigma(EM(x, y, t)). \quad (1)$$

The coefficient of variance (CoV) is calculated as the standard deviation across the ensemble members divided by the ensemble mean,

$$CoV(x,y,t) = \frac{\sigma(EM(x,y,t))}{\overline{LE}}. \quad (2)$$

The forced response of the large ensemble is calculated as the mean of ensemble members at a given location and time,

$$\overline{LE}(x,y,t) = \frac{\sum_1^n EM(x,y,t)}{n}, \quad (3)$$

where n is the number of ensemble members.

We quantified the relationship between phytoplankton carbon variance and the variables which contribute to changing phytoplankton biomass variance by performing a multiple linear regression (MLR) analysis. The MLR analysis was performed on linearly detrended annual anomalies using the ordinary least squares function of the Python package statsmodel.api. We reconstructed the contribution of each variable to phytoplankton biomass variance between the beginning (2006 to 2016) and end (2090 to 2100) of the century by multiplying the MLR regression coefficients by the 10-year averaged standard deviation across the model ensemble (ensemble spread) for each variable. We reconstruct phytoplankton biomass variance ($\sigma_{C_{phyto}}$) as a function of light ($Solar$), temperature (SST), phosphate advection ($Nutrient$), mixed layer depth (MLD), and zooplankton grazing ($Grazing$),

$$\sigma_{C_{phyto}} = \frac{\partial C_{phyto}}{\partial Solar}\sigma_{Solar} + \frac{\partial C_{phyto}}{\partial SST}\sigma_{SST} + \frac{\partial C_{phyto}}{\partial Nutrient}\sigma_{Nutrient} + \frac{\partial C_{phyto}}{\partial MLD}\sigma_{MLD} + \frac{\partial C_{phyto}}{\partial Grazing}\sigma_{Grazing}, \quad (4)$$

where σ_X represents the 10-year average of the standard deviation across all ensemble members for a particular variable and $\frac{\partial C_{phyto}}{\partial X}$ represents the MLR regression coefficient describing the relationship between a particular variable and phytoplankton biomass variance. We approximate at first-order the linear relationships between variables and do not account for second-order (co-variance among explanatory variables) relationships in our statistical method; these terms do not contribute much to the total change in variance (Figure S3).

2.2 Model Evaluation

We used remotely sensed estimates of phytoplankton carbon to evaluate the representation of phytoplankton interannual variability in the CESM1-LE. In other words, we evaluate the temporal variability in modeled phytoplankton biomass from year to year. We note that this interannual variability is different than the internal variability (ensemble spread) that we discuss at length in this study, but is nevertheless a target for model validation. Although phytoplankton carbon concentrations cannot be measured directly by satellites, they can be reconstructed using algorithms that incorporate remotely sensed chlorophyll concentrations, detrital backscattering coefficients, and phytoplankton absorption (Kostadinov et al., 2016; Martinez-Vicente

et al., 2017; Roy et al., 2017; Sathyendranath et al., 2020; Brewin et al., 2021). We use the observational phytoplankton carbon dataset of Bellacicco et al. (2020), annually averaged and interpolated onto a 1° grid, to evaluate temporal variability in phytoplankton biomass in a single model ensemble member. Figure 1a shows satellite derived estimates of interannual variability in phytoplankton carbon with regions of relatively low phytoplankton variability shown in ~~light green~~ yellow and regions of relatively high variability in ~~dark blue~~purple. Remotely sensed observations capture areas of high interannual variability in the subpolar North Atlantic, North Pacific, and Southern Ocean and areas of low interannual variability in the subtropical gyre regions. Similar spatial patterns are apparent when compared to the range of phytoplankton interannual variability in ensemble member 1 of the CESM1-LE over the observational period (1998 to 2019) (Figure 1b). However, while the model ensemble captures regional patterns of observed variability, the CESM1-LE overestimates the magnitude of observed interannual variability. ~~As such, estimates of interannual variability derived from the model ensemble will tend to overestimate that observed in the real world~~Some regions of the global ocean display a substantial mismatch in temporal variability between the model and that estimated from observations (Figure 1,Table S1). While the differences can be quite large in some regions, we note that this is an evaluation of temporal variability (rather than internal variability, the focus of this study), and that estimates from the satellite product derive from a collection of data products which may also display biases (Table S1).

As an evaluation of the model's ability to represent internal variability (ensemble spread), we compare the internal variance in chlorophyll simulated in the CESM1-LE to a synthetic ensemble generated from observed chlorophyll concentrations over the MODIS remote sensing record (Elsworth et al., 2020, 2021) (Figure ~~S2~~S4; chlorophyll was readily available in the CESM1-LE and can be directly compared with our synthetic ensemble of observed chlorophyll). A synthetic ensemble is a ~~novel~~ technique that allows the observational record to be statistically emulated to create multiple possible evolutions of the observed record, each with a unique sampling of internal climate variability (McKinnon et al., 2017; McKinnon and Deser, 2018). Compared to the internal variability over the observational period (2002 to 2020) (purple circle, (Figure ~~S2~~S4), the model ensemble slightly overestimates the magnitude of internal variability in chlorophyll observed in the real world.

Taken together, our model validation exercises demonstrate that the model tends to overestimate both the temporal (interannual) variability and the internal variability in phytoplankton, as compared to satellite observations on both global and regional scales. Thus, we must interpret our findings with this caveat in mind. The change in variance that we model is likely an upper-end estimate.

3 Results

We evaluate the change in mean phytoplankton biomass and its variance across in the CESM1-LE globally and regionally. Annually averaged, global mean, upper-ocean (top 150m) integrated phytoplankton biomass across the model ensemble decreases from 76.1 mmol C m^{-2} to 66.2 mmol C m^{-2} from the historical period through the RCP8.5 forcing scenario (1920 to 2100), a decline of 13% (black curve; Figure 2a). The change in the mean is calculated as the difference between the first (1920 to 1930) and last (2090 to 2100) decades across the historical and RCP8.5 forcing scenario. Phytoplankton biomass declines globally, except in polar regions (Figure 3a). Regional changes in mean phytoplankton biomass across the RCP8.5 forcing

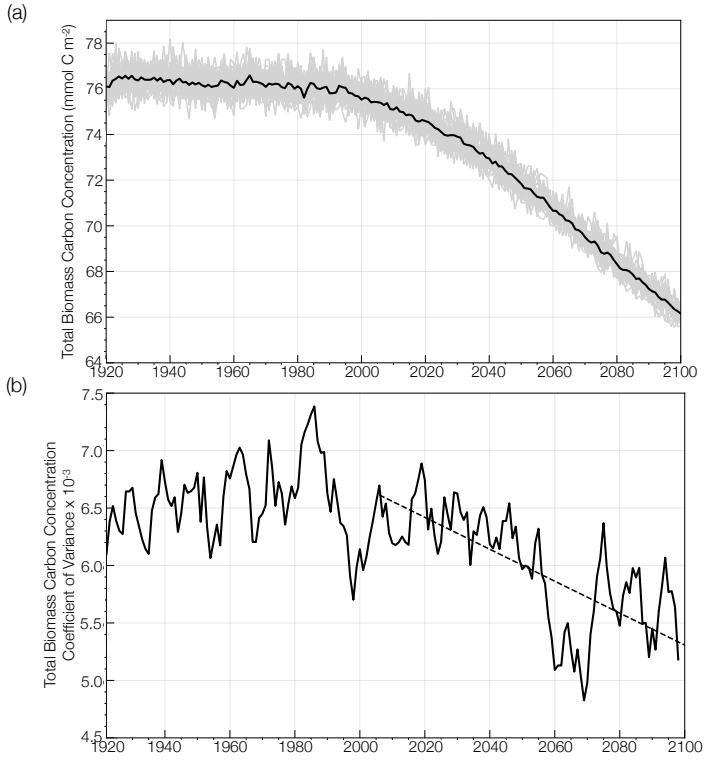

Figure 2. (a) Global change in annual mean total phytoplankton carbon concentration simulated by the CESM1-LE in mmol C m^{-2} from the historical period through the RCP8.5 forcing scenario (1920 to 2100). The ensemble mean is shown in the black curve and the 34 individual ensemble members are shown in the gray curves. (b) Global change in the coefficient of variance in annual mean total phytoplankton carbon concentration over the same period, smoothed using a 5 year window. Trend in the coefficient of variance over the RCP8.5 forcing scenario is shown in the black dashed line.

scenario (2006 to 2100) display increasing biomass in portions of the Arctic and the Southern Ocean that gradually become ice-free over the century (on the order of 20-40% of the mean biomass across the century) and decreasing biomass across the subtropical gyres (on the order of 15-30% of the mean biomass across the century; Figures 3a, ~~S4~~S5a). In the North Atlantic subpolar gyre, the phytoplankton biomass declines by 40-50% of its mean (Figures 3a, ~~S4a), likely due to weakening of the Atlantic Meridional Overturning Circulation (AMOC) and the subsequent disruption of nutrient flux (?)~~S5a). This result is consistent with previous modelling studies which identified a 50% reduction in North Atlantic primary production associated with AMOC weakening during the last glacial period (Schmittner, 2005). A weakening of the AMOC is also projected with anthropogenic warming (Manabe and Ronald, 1993; Stocker and Schmittner, 1997).

Regional changes in phytoplankton biomass are dominated by changes in diatom and small phytoplankton (Table 1). We aggregate biomass across 11 ecological provinces (Vichi et al., 2011; Tagliabue et al., 2021), and present changes in total and PFT biomass over the RCP8.5 scenario in Table 1. The CESM1-LE simulates the largest decline in total phytoplankton

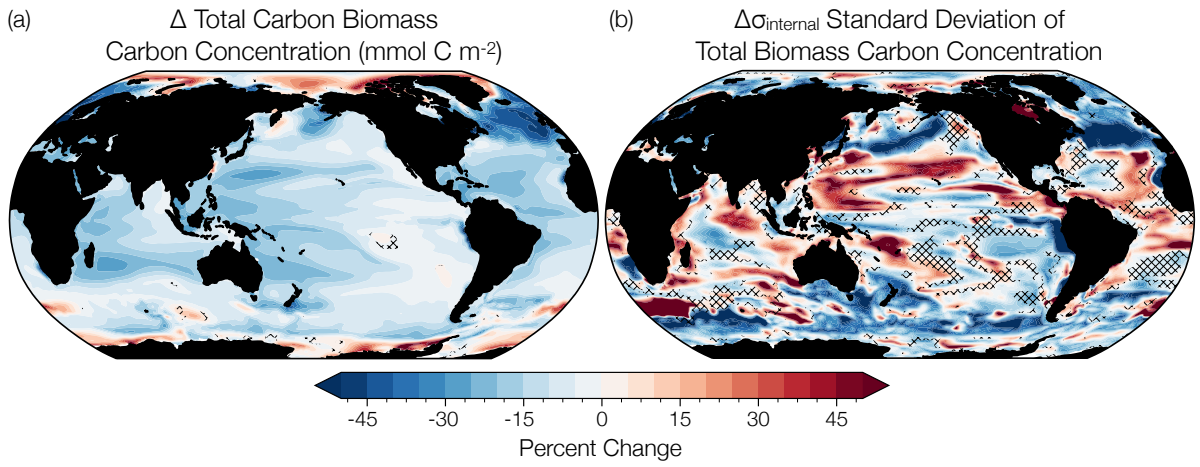

Figure 3. (a) Percentage change in annual total phytoplankton carbon concentration over the RCP8.5 forcing scenario (2006 to 2100) simulated by the CESM1-LE. (b) Percentage change in annual total phytoplankton variablity over the same period. Hatched areas indicate regions of trend insignificance determined by a t-test with a p value greater than 0.05. The change in the mean and the variability are calculated using averages across the first (2006 to 2016) and last (2090 to 2100) decades of the RCP8.5 forcing scenario.

carbon concentration in the Atlantic subpolar (ASP) region, where diatom biomass declines by ∼80 mmol C m^{-2}, and small phytoplankton biomass increases slightly (∼8 mmol C m^{-2}). We observe moderate decreases in the subpolar Pacific (SAP) region that are again driven by declines in diatom carbon concentration, with minor contributions from changes in small phytoplankton carbon concentration (Table 1). The CESM1-LE simulates a smaller decline in total carbon concentration in the Equatorial Pacific (EQP) region, where diatom biomass declines ∼7 mmol C m^{-2} and small phytoplankton biomass declines ∼5 mmol C m^{-2}. The smallest decline in total carbon concentration occurs in the South Pacific subtropical gyre (SPS) region, where diatom biomass declines ∼4.3 mmol C m^{-2} and small phytoplankton biomass declines ∼4.6 mmol C m^{-2}.

Internal variability in global phytoplankton biomass, which is indicated by the spread across the individual ensemble members (gray lines; Figure 2a), declines over the RCP8.5 forcing period from 2006 to 2100. To quantify how the range of internal variability in phytoplankton biomass is changing with anthropogenic warming, we calculated the coefficient of variance as the standard deviation across the ensemble members for a given year (ensemble spread) divided by the ensemble mean. Figure 2b illustrates the change in the coefficient of variance from the historical period through the RCP8.5 forcing scenario (1920 to 2100). The coefficient of variance is relatively constant across the historical period (1920 to 2005), and then significantly declines by ∼20% from 2006-2100.

A decrease in global phytoplankton internal variability with anthropogenic warming is not unique to the CESM1-LE. We illustrate this by analyzing phytoplankton chlorophyll (rather than biomass; chlorophyll was readily available in the CMIP5 archive) from three other CMIP5 ESM large ensembles which include representation of ocean biogeochemistry: the GFDL-ESM2M from the Geophysical Fluid Dynamics Laboratory (GFDL; Dunne et al., 2012, 2013), the CanESM2 from the Cana-

dian Centre for Climate Modelling and Analysis (Christian et al., 2010; Arora et al., 2011), and the MPI-ESM-LR from the Max Planck Institute (MPI; Giorgetta et al., 2013; Ilyina et al., 2013), consisting of 30, 50, and 100 ensemble members, respectively. Similarly to the CESM1-LE, historical forcing was applied through 2005, followed by RCP8.5 forcing through 2100. While there is substantial spread in the mean coefficient of variance across the four models, a similar decline in the coefficient of variance can be observed across each of the four ESM ensembles, (Figure ~~S2~~S4). From 2006 to 2100, the coefficient of variance decreases by 3.3×10^{-5} yr^{-1} in the CESM1-LE, 2.0×10^{-4} yr^{-1} in the MPI-ESM-LR1, 5.2×10^{-5} yr^{-1} in the CanESM2, and 3.9×10^{-4} yr^{-1} in the GFDL-ESM2M. The change in the coefficient of variance is calculated using averages across the first (2006 to 2016) and last (2090 to 2100) decades of the RCP8.5 forcing scenario. These declines are statistically significant in all model ensembles with the exception of the MPI-ESM-LR1 (Figure ~~S2~~S4).

In comparison to the mean change in phytoplankton biomass, changes in phytoplankton internal variability with time are spatially more heterogeneous across the global ocean (Figure 3b). The largest decreases in variance are apparent in the North Atlantic and North Pacific subpolar regions (on the order of 50-70% of the mean biomass variance), with smaller declines in the Equatorial Pacific and Southern Oceans (on the order of 30-50% of the mean biomass variance) (Figure 3b, ~~S4~~S5b). Changes in variance in the subtropical regions are characterized by mixed trends, with areas of both increasing and decreasing variance across the RCP8.5 forcing scenario (Figure 3b, ~~S4~~S5b).

Global changes in total phytoplankton biomass ~~variance~~ standard deviation are a manifestation of changes in diatom and small phytoplankton variability (Table 1). We observe the largest magnitude decline in total phytoplankton carbon ~~variance~~ standard deviation in the subpolar Atlantic (ASP) region, where diatom ~~variance~~ standard deviation declines by $\sim$10 mmol C m^{-2} and small phytoplankton ~~variance~~ standard deviation declines by $\sim$2 mmol C m^{-2} (Table 1). The CESM1-LE simulates a moderate magnitude decline in total phytoplankton ~~variance~~ standard deviation in the subarctic Pacific (SAP) region, driven by a decrease in small phytoplankton ~~variance~~ standard deviation ($\sim$2 mmol C m^{-2}) with minor contributions from declines in diatom ~~variance~~ standard deviation ($\sim$1 mmol C m^{-2}) (Table 1). Moderate declines in ~~variance~~ standard deviation are also simulated in the Arctic (ARC), North Atlantic subtropical gyre (NAS), Southern Ocean (SOC), and Equatorial Pacific (EQP) regions, driven by declines in diatom carbon ~~variance~~ standard deviation in the SOC region and declines in small phytoplankton variance in the EQP region (Table 1).

To guide our ~~attribution~~ analysis of changing phytoplankton biomass ~~and its~~ internal variability, we considered the dominant ecological assemblage across different regions of the global ocean. The CESM1-LE simulates three phytoplankton functional types, each of which thrive in distinct regions of the global ocean. Diatoms dominate in the subpolar Atlantic and Pacific, the Eastern Equatorial upwelling zone, and portions of the Southern Ocean, while small phytoplankton dominate across the subtropical gyres and portions of the Southern Ocean (Figure 4). In contrast, diazotrophs, a minor contributor to total carbon biomass, are present at such low concentrations that they do not dominate anywhere in the global ocean (Figure 4). Using the ecologically cohesive regions defined by Tagliabue et al. (2021) and Vichi et al. (2011), we selected areas that align with the most productive fisheries regions by catch in the Atlantic and Pacific basins (FAO, 2020), as well as regions of global biogeochemical importance for further analysis. In each ecological region we identified the dominant phytoplankton functional

Table 1. Changes in phytoplankton biomass and its variability in the CESM1-LE from 2006 to 2100 for the 11 ecological provinces defined in Vichi et al. (2011) and Tagliabue et al. (2021). Units are mmol C m^{-2}. The change in the mean and standard deviation are calculated using averages across the first (2006 to 2016) and last (2090 to 2100) decades of the RCP8.5 forcing scenario.

Region		Change in Mean			Change in Standard Deviation		
Biome	Name	Total	Diatom	Small	Total	Diatom	Small
ARC	Arctic	–21	–58	+37	–1.4	–2.8	–0.3
ASP	Atlantic subpolar	–71	–79	+8.2	–5.6	–9.9	–2.2
NAS	North Atlantic subtropical gyre	–18	–15	–2.9	–1.8	–2.8	–0.3
EQA	Equatorial Atlantic	–12	–6.6	–5.9	–0.1	–0.4	+0.2
SAS	South Atlantic subtropical gyre	–10	–7.2	–3.1	–0.5	–0.6	–0.1
IND	Indian Ocean	–11	–6.1	–4.7	+0.1	0	+0.1
SAP	subarctic Pacific	–21	–15	–5.4	–0.1	–1.4	–2.4
NPS	North Pacific subtropical gyre	–11	–5.6	–4.9	–0.2	–0.4	+0.1
EQP	Equatorial Pacific	–12	–6.6	–5.0	–2.0	–2.0	–0.2
SPS	South Pacific subtropical gyre	–8.9	–4.3	–4.6	–0.1	0	–0.1
SOC	Southern Ocean	–9.3	–2.8	–6.6	–1.0	0	–1.3

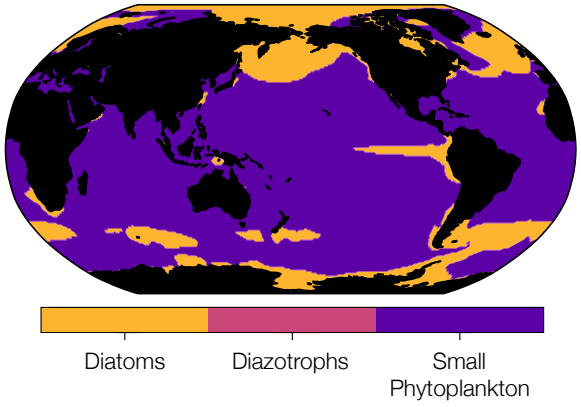

Figure 4. Distribution of the dominant phytoplankton functional type in biomass carbon averaged ~~over~~ across the RCP8.5 forcing scenario (2006 to ~~2100.~~ 2100). The CESM1-LE simulates three phytoplankton functional types: diatoms, diazotrophs, and small phytoplankton. Regions where diatoms dominate are shown in yellow, regions where diazotrophs dominate are shown in pink, and regions where small phytoplankton dominate are shown in purple.

type to include in our ~~driver~~ analysis. In regions where multiple phytoplankton functional types dominated, we used total carbon concentrations to reflect the mixed ecological assemblage.

We ~~quantified the relationship between phytoplankton carbon and the variables which contribute to changing phytoplankton biomass and its internal variability by performing a multiple linear regression (MLR) analysis. The MLR analysis was performed on linearly detrended annual anomalies using the ordinary least squares function of the Python package statsmodels.api. We then reconstructed the contribution of each driver variable to phytoplankton biomass and its internal variance between the beginning of the century (2006~~ identify the contribution to ~~2016) and the end of the century (2090 to 2100) by multiplying the MLR regression coefficients by the 10-year averaged mean and standard deviation across the model ensemble (ensemble spread), respectively, for each variable. We reconstruct mean phytoplankton biomass ($\overline{C_{phyto}}$) and its variance ($\sigma_{C_{phyto}}$) as a function of light ($Solar$), temperature (SST), phosphate advection ($Nutrient$), mixed layer depth (MLD), and zooplankton grazing ($Grazing$),~~

$$\overline{C_{phyto}} = \frac{\partial C_{phyto}}{\partial Solar}\overline{Solar} + \frac{\partial C_{phyto}}{\partial SST}\overline{SST} + \frac{\partial C_{phyto}}{\partial Nutrient}\overline{Nutrient} + \frac{\partial C_{phyto}}{\partial MLD}\overline{MLD} + \frac{\partial C_{phyto}}{\partial Grazing}\overline{Grazing},$$

~~and,~~

$$\sigma_{C_{phyto}} = \frac{\partial C_{phyto}}{\partial Solar}\sigma_{Solar} + \frac{\partial C_{phyto}}{\partial SST}\sigma_{SST} + \frac{\partial C_{phyto}}{\partial Nutrient}\sigma_{Nutrient} + \frac{\partial C_{phyto}}{\partial MLD}\sigma_{MLD} + \frac{\partial C_{phyto}}{\partial Grazing}\sigma_{Grazing},$$

~~where $\overline{X}$ represents the 10-year ensemble mean for a particular variable over a given period, σ_X represents the standard deviation across all ensemble members for a particular variable and $\frac{\partial C_{phyto}}{\partial X}$ represents the MLR regression coefficient describing the relationship between a particular variable and phytoplankton biomass. We approximate at first-order the linear relationships between variables and do not account for second-order (co-variance among explanatory variables) relationships in our statistical method; these terms do not contribute much to the total change in mean (Figure S7a) and variance (Figure S7b).~~

~~We identify the drivers of~~ changing phytoplankton biomass ~~and its~~ internal variance in four distinct ecological regions using our statistical approach. In the subpolar Atlantic (ASP) and subpolar Pacific (SAP) ecological provinces ~~, where diatoms dominate total biomass, the mean decline in diatom carbon is associated with a decrease in diatom grazing~~ (Figure ~~S3a) and a decrease zooplankton carbon, respectively (Figure S3b). In the ASP and SAP ecological provinces (Figure~~ 4), diatom variance declines between the beginning and end of the century (Figure 5a, b, Table 1). In both provinces, the largest contributions to this decline in diatom variability derive from a decline in diatom grazing variability, while more minor contributions derive from bottom-up controls such as solar flux, sea surface temperature, nutrient advection, and mixed layer depth (Figure 5a, b).

As the Southern Ocean (SOC) and Equatorial Pacific (EQP) provinces are characterized by mixed phytoplankton assemblages where both diatoms and small phytoplankton dominate, we identify the ~~drivers of~~ contributions to the change in total phytoplankton ~~mean and~~ variance here. ~~The mean decline in total carbon in the SOC province are dominated by a decrease zooplankton grazing (Figure S3c). In contrast , drivers of the mean decline in total carbon in the EQP province include a combination of zooplankton carbon, diatom grazing, and small phytoplankton grazing (Figure S3d).In contrast to the ASP and SAP~~ In contrast to the subpolar Atlantic and subpolar Pacific provinces, we observe a relatively smaller decline in internal

phytoplankton variance between the beginning and end of the century in the Southern ocean (Figure 5c). Similarly to ~~ASP and SAP~~ the subpolar Atlantic and subpolar Pacific provinces, the largest contributions to the change in internal variability derive from a decline in grazing variability, with bottom-up controls playing only a small role (Figure 5c). In the Equatorial Pacific, total phytoplankton variance declines between the beginning and end of the century, with the largest contributions to this decline deriving from zooplankton carbon and diatom grazing, with increasing variance in small phytoplankton grazing (Figure 5d).

We explore the sensitivity of our results in relation to the functional form of grazing in the CESM1-LE (Figure ~~S5~~S6). A caveat to our statistical approach is our assumption that the regression coefficients are constant across the century while the variance is changing. In our model, the sensitivity of grazing rate to prey concentration can be affected by changes in prey concentration and changes in temperature (Figure S1), both of which are modified in a changing climate. We test the robustness of our assumption in the two key fisheries regions by performing another MLR to reconstruct ~~drivers of~~ contributions to diatom variance with different regression coefficients between the beginning and end of the century (Figure S1, Figure ~~S5~~S6). While the contribution of zooplankton grazing to the change in diatom variance changes slightly with this new approach, the results are similar.

The declining internal variance in phytoplankton biomass co-occurs with a reduction in zooplankton grazing variability. Our analysis reveals that changes in grazer variance dominate the change in phytoplankton variance over the next century, so we next deconvolve the changes in grazer variance into its two ~~drivers~~components, prey concentration (phytoplankton biomass) and temperature (Figure S1) using a similar MLR approach as for phytoplankton biomass variance (e.g., Equation 4). The results of this deconvolution (Figure ~~??~~S8) demonstrate that the changing grazing variance is driven primarily by changing phytoplankton biomass variance, with only small contributions from changing temperature variance. Thus, it is not possible to cleanly separate cause and effect in this non-linear, coupled system: phytoplankton variance changes because grazer variance changes, and grazer variance changes because phytoplankton variance changes. Nevertheless, our results suggest that both phytoplankton and zooplankton experience declines in variance by the end of the century, and as both are sources of energy for higher trophic levels, this implies that fishery productivity variance will also decline by the end of the century.

4 Conclusions and Discussion

We quantify both global and regional changes in phytoplankton internal variance across the RCP8.5, or business-as-usual forcing scenario in the CESM1-LE. We observe a global decline in phytoplankton variance in the model ensemble, which is reflected in similar declines in phytoplankton variance across a suite of CMIP5 models (Figure ~~S2~~S4). Regional changes in phytoplankton variability with anthropogenic climate change in the model ensemble are spatially heterogeneous, with highly productive fisheries regions and important global biogeochemical regions experiencing large changes in variance. Statistical analysis of these specific regions reveal ~~zooplankton grazing (top-down control) as an important contributor to changes in phytoplankton variance~~the decline in phytoplankton biomass variance to co-occur with a reduction in zooplankton grazing variability, consistent with previous studies (Bopp et al., 2001; Laufkötter et al., 2015).

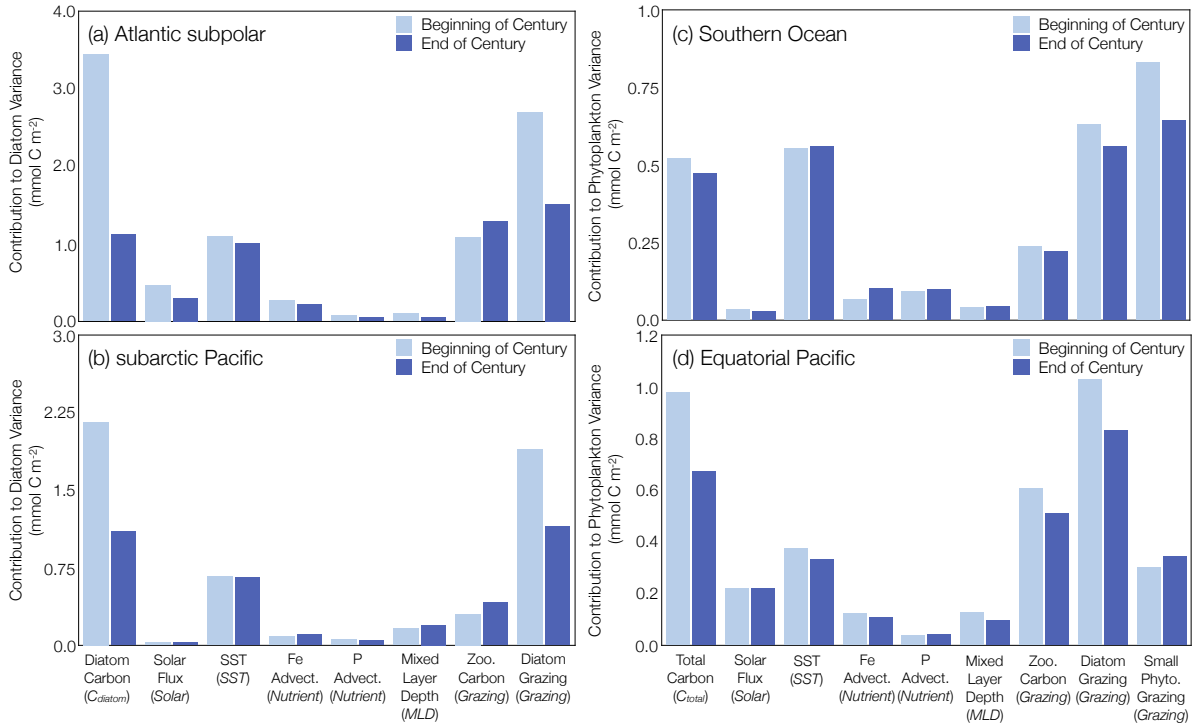

Figure 5. Reconstructed changes in the contribution of each ~~driver~~ variable to phytoplankton biomass ~~variance~~ standard deviation across the RCP8.5 forcing scenario (2006 to 2100) with the beginning of the century shown in light blue and the end of the century shown in dark blue. Marine ecological regions are defined in Tagliabue et al. (2021). Regions were selected which aligned with the highest fisheries catch in the (a) Atlantic and (b) Pacific basins and the biogeochemically important (c) Southern Ocean and (d) Equatorial Pacific regions. The dominant phytoplankton functional type is considered in each region. In regions with a mixed ecological assemblage, total phytoplankton carbon is considered. The change in the coefficient of variance is calculated using averages across the first (2006 to 2016) and last (2090 to 2100) decades of the RCP8.5 forcing scenario.

While the CESM1-LE represents ~~regional patterns~~ the overall spatial pattern of observed interannual variability in phytoplankton carbon, the model ~~ensemble tends to slightly overestimate~~ overestimates the magnitude of observed interannual and internal variance in phytoplankton ~~chlorophyll~~on regional scales. As such, the magnitude of changes in phytoplankton internal variance derived from the model ensemble should be interpreted as an overestimate when considering changes in phytoplankton internal variance driven by anthropogenic warming. This caveat is particularly important to consider when interpreting projections from offline fisheries models in the context of fisheries adaptation and planning in a warming climate.

Our statistical approach has inherent limitations, especially in the context of a attributing ~~drivers~~ contributory variables in an inherently non-linear, coupled system (i.e., reconstructing linear relationships between co-varying variables). In a coupled system such as this, it is difficult to definitively identify cause and effect. In this context, the statistical method can be used as an effective tool to provide a first-order approximation of ~~drivers of~~ contributions to phytoplankton variance across the century.

While many studies attribute bottom-up controls to changing phytoplankton with anthropogenic warming (Steinacher et al., 2010; Bopp et al., 2013; Lotze et al., 2019; Tittensor et al., 2021), top-down controls may also play an important role, particularly in our understanding of changing phytoplankton biomass and its variance. Our study demonstrates a ~~key role for top-down controls on changing phytoplankton biomass and its~~ strong connectivity between phytoplankton and zooplankton grazing variance in the subpolar North Atlantic and subpolar North Pacific. Previous studies of phytoplankton change with climatic warming have demonstrated that grazing pressure is a ~~driver of~~ contributor to biomass decline in low to intermediate latitude regions across a suite of model simulations with different marine ecosystem models (Laufkötter et al., 2015) and that top-down controls can affect regional changes in NPP and export production (Bopp et al., 2001) and is a ~~driver of~~ contributor to future shifts in bloom timing (Yamaguchi et al., 2022). While grazing pressure has been shown to increase in response to climate change, several ecosystem models have also identified zooplankton grazing as a dominant ~~driver of~~ contributor to phytoplankton assemblage succession during blooms (Hashioka et al., 2012; Prowe et al., 2012a). Additionally, top-down controls have also been observed to affect the onset of the spring bloom (Behrenfeld, 2010; Behrenfeld et al., 2013), to influence primary production in a trait-based ecosystem model (Prowe et al., 2012b).

The relative simplicity of the ocean biogeochemical ecosystem model in CESM1 (e.g., representation of a single zooplankton functional type with multiple grazing rates) may limit a more detailed evaluation of changing grazing pressures with climate change. While the recent parameterization of the biogeochemical ecosystem model in CESM2 (MARBL) includes similar representation of three PFTs and a single adaptive ZFT (Long et al., 2021), more complex configurations of MARBL include explicit representation of additional PFTs such as coccolithophores (Krumhardt et al., 2019) and ZFTs. Using more complex ecosystem models, additional insights into ~~drivers of~~ contributions to variability may be gained using our statistical approach. Additionally, the use of an ecosystem model of higher complexity may provide more realistic projections of the marine ecosystem with climate change considering change in phytoplankton and zooplankton species diversity with anthropogenic warming (Benedetti et al., 2021). However, our regional analyses suggest that ~~zooplankton grazing pressure should be considered as an important driver of changes in phytoplankton biomass and its variance~~ both phytoplankton and zooplankton grazing variance are likely to change with anthropogenic warming.

The magnitude and direction of regional changes in phytoplankton variance are an essential constraint for near-term (subseasonal to decadal) predictions of the local marine ecosystem, particularly in important fisheries regions such as the subpolar Atlantic (ASP) and the subpolar Pacific (SAP) ecological provinces (FAO, 2020). Accurate near-term predictions require foreknowledge of both internal climate variability and external climate change signals. On subseasonal to decadal timescales, the magnitude of internal climate variability is often stronger than forced climate change signals (Meehl et al., 2009, 2014). In this context, a decline in phytoplankton internal variance with anthropogenic climate change may improve the accuracy of near-term predictions of phytoplankton biomass, producing more reliable forecasts of fisheries productivity. Future work can utilize these constraints on phytoplankton variance, particularly on regional scales, to inform climate mitigation and adaptation efforts.

Author contributions. GE and NL conceptualized the study. GE analyzed simulation results and prepared the manuscript. N.L. assisted in preparing the manuscript. KK assisted in analysis of simulation results. TM, KK, and SS assisted in reviewing the manuscript.

Acknowledgements. Computational resources were provided by the Computational and Information Systems Laboratory (CISL) at the National Center for Atmospheric Research (NCAR), through a resource allocation to GWE and NSL. GWE and NSL are grateful for support from the National Science Foundation (NSF) (OCE-1558225, OCE-1752724).

References

Arora, V., Scinocca, J., Boer, G., Christian, J., Denman, K., Flato, G., Kharin, V., Lee, W., and Merryfield, W.: Carbon emission limits required to satisfy future representative concentration pathways of greenhouse gases, Geophysical Research Letters, 38, doi:10.1029/2010GL046270, 2011.

Behrenfeld, M.: Abandoning Sverdrup's Critical Depth Hypothesis on phytoplankton blooms, Ecology, 91, 977–89, doi:10.1890/09-1207.1, 2010.

Behrenfeld, M., Doney, S., Lima, I., Boss, E., and Siegel, D.: Annual cycles of ecological disturbance and recovery underlying the subarctic Atlantic spring plankton bloom: PHYTOPLANKTON BLOOMS, Global Biogeochemical Cycles, 27, doi:10.1002/gbc.20050, 2013.

Bellacicco, M., Pitarch, J., Organelli, E., Martinez-Vicente, V., Volpe, G., and Marullo, S.: Improving the Retrieval of Carbon-Based Phytoplankton Biomass from Satellite Ocean Colour Observations, Remote Sensing, 12, 3640, doi:10.3390/rs12213640, 2020.

Benedetti, F., Vogt, M., Hofmann Elizondo, U., Righetti, D., Zimmermann, N., and Gruber, N.: Major restructuring of marine plankton assemblages under global warming, Nature Communications, 12, doi:10.1038/s41467-021-25385-x, 2021.

Blanchard, J., Jennings, S., Holmes, R., Harle, J., Merino, G., Allen, I., Holt, J., Dulvy, N., and Barange, M.: Potential consequences of climate change on primary production and fish production in large marine ecosystems, Philosophical Transactions of the Royal Society B, 367, 2979–2989, doi:10.1098/rstb.2012.0231, 2012.

Blanchard, J., Watson, R., Fulton, E., Cottrell, R., Nash, K., Bryndum-Buchholz, A., Büchner, M., Carozza, D., Cheung, W., Elliott, J., Davidson, L., Dulvy, N., Dunne, J., Eddy, T., Galbraith, E., Lotze, H., Maury, O., Müller, C., Tittensor, D., and Jennings, S.: Linked sustainability challenges and trade-offs among fisheries, aquaculture and agriculture, Nature, 1, doi:10.1038/s41559-017-0258-8, 2017.

Bopp, L., Monfray, P., Aumont, O., Dufresne, J.-L., Treut, H., Madec, G., Terray, L., and Orr, J.: Potential impact of climate change on marine export production, Global Biogeochemical Cycles, 15, 81–100, doi:10.1029/1999GB001256, 2001.

Bopp, L., Resplandy, L., Orr, J., Doney, S., Dunne, J., Gehlen, M., Halloran, P., Heinze, C., Ilyina, T., Séférian, R., Tjiputra, J., and Vichi, M.: Multiple stressors of ocean ecosystems in the 21st century: Projections with CMIP5 models, Biogeosciences, 10, 6225–6245, doi:10.5194/bg-10-6225-2013, 2013.

Bopp, L., Aumont, O., Kwiatkowski, L., Clerc, C., Dupont, L., Ethé, C., Séférian, R., and Tagliabue, A.: Diazotrophy as a key driver of the response of marine net primary productivity to climate change, Biogeosciences, doi:10.5194/bg-2021-320, 2021.

Brewin, B., Sathyendranath, S., Platt, T., Bouman, H., Ciavatta, S., Dall'Olmo, G., Dingle, J., Groom, S., Jönsson, B., Kostadinov, T., Kulk, G., Laine, M., Martinez-Vicente, V., Psarra, S., Raitsos, D., Richardson, K., Rio, M.-H., Rousseaux, C., Salisbury, J., and Walker, P.: Sensing the ocean biological carbon pump from space: A review of capabilities, concepts, research gaps and future developments, Earth-Science Reviews, 217, 103 604, doi:10.1016/j.earscirev.2021.103604, 2021.

Cai, W., Borlace, S., Lengaigne, M., Rensch, P., Collins, M., Vecchi, G., Timmermann, A., Santoso, A., McPhaden, M., Wu, L., England, M., Wang, G., Guilyardi, E., and Jin, F.-F.: Increasing frequency of extreme El Niño Events due to greenhouse warming, Nature Climate Change, 4, 111–116, doi:10.1038/nclimate2100, 2014.

Cai, W., Wang, G., Santoso, A., McPhaden, M., Wu, L., Jin, F.-F., Timmermann, A., Collins, M., Vecchi, G., Lengaigne, M., England, M., Dommenget, D., Takahashi, K., and Guilyardi, E.: Increased frequency of extreme La Niña Events under greenhouse warming, Nature Climate Change, 5, 132–137, doi:10.1038/nclimate2492, 2015.

Cai, W., Ng, B., Wang, G., Santoso, A., Wu, L., and Yang, K.: Increased ENSO sea surface temperature variability under four IPCC emission scenarios, Nature Climate Change, doi:10.1038/s41558-022-01282-z, 2022.

Chassot, E., Bonhommeau, S., Dulvy, N., Mélin, F., Watson, R., and le pape, O.: Global marine primary production constrains fisheries catches, Ecology Letters, 13, 495 – 505, doi:10.1111/j.1461-0248.2010.01443.x, 2010.

Cheung, W., Lam, V., Sarmiento, J., Kearney, K., Watson, R., and Pauly, D.: Projecting Global Marine Biodiversity Impacts under Climate Change Scenarios, Fish and Fisheries, 10, 235 – 251, doi:10.1111/j.1467-2979.2008.00315.x, 2009.

Cheung, W., Lam, V., Sarmiento, J., Kearney, K., Watson, R., Zeller, D., and Pauly, D.: Large-scale Redistribution of Maximum Fisheries Catch Potential in the Global Ocean under Climate Change, Global Change Biology, 16, 24 – 35, doi:10.1111/j.1365-2486.2009.01995.x, 2010.

Christensen, V. and Walters, C.: Ecopath With Ecosim: Methods, Capabilities and Limitations, Ecological Modelling, 172, 109–139, doi:10.1016/j.ecolmodel.2003.09.003, 2004.

Christensen, V., Coll, M., Buszowski, J., Cheung, W., Frölicher, T., Steenbeek, J., Stock, C., Watson, R., and Walters, C.: The global ocean is an ecosystem: Simulating marine life and fisheries, Global Ecology and Biogeography, 24, doi:10.1111/geb.12281, 2015.

Christian, J., Arora, V., Boer, G., Curry, C., Zahariev, K., Denman, K., Flato, G., Lee, W., Merryfield, W., Roulet, N., and Scinocca, J.: The global carbon cycle in the Canadian Earth system model (CanESM1): Preindustrial control simulation, Journal of Geophysical Research (Biogeosciences), 115, doi:10.1029/2008JG000920, 2010.

Danabasoglu, G., Bates, S. C., Briegleb, B. P., Jayne, S. R., Jochum, M., Large, W. G., Peacock, S., and Yeager, S. G.: The CCSM4 ocean component, Journal of Climate, 25, 1361–1389, doi:10.1175/JCLI-D-11-00091.1, 2012.

Deser, C., Phillips, A., Bourdette, V., and Teng, H.: Uncertainty in climate change projections: The role of internal variability, Climate Dynamics, 38, 527–546, doi:10.1007/s00382-010-0977-x, 2010.

Deser, C., Knutti, R., Solomon, S., and Phillips, A.: Communication of the role of natural variability in future North American climate, Nature Climate Change, 2, 775–779, doi:10.1038/nclimate1562, 2012.

Doney, S., Lindsay, K., Fung, I., and John, J.: Natural variability in a stable, 1000-Yr global coupled climate–carbon cycle simulation, Journal of Climate, 19, 3033–3054, doi:10.1175/JCLI3783.1, 2006.

Dunne, J., John, J., Adcroft, A., Griffies, S., Hallberg, R., Shevliakova, E., Ronald, S., Cooke, W., Dunne, K., Harrison, M., Krasting, J., Malyshev, S., Milly, P., Phillips, P., Sentman, L., Samuels, B., Spelman, M., Winton, M., Wittenberg, A., and Zadeh, N.: GFDL's ESM2 Global Coupled Climate–Carbon Earth System Models. Part I: Physical Formulation and Baseline Simulation Characteristics, Journal of Climate, 25, 6646–6665, doi:10.1175/JCLI-D-11-00560.1, 2012.

Dunne, J., John, J., Shevliakova, E., Ronald, S., Krasting, J., Malyshev, S., Milly, P., Sentman, L., Adcroft, A., Cooke, W., Dunne, K., Griffies, S., Hallberg, R., Harrison, M., Levy, H., Wittenberg, A., Phillips, P., and Zadeh, N.: GFDL's ESM2 Global Coupled Climate–Carbon Earth System Models. Part II: Carbon System Formulation and Baseline Simulation Characteristics*, Journal of Climate, 26, 2247–2267, doi:10.1175/JCLI-D-12-00150.1, 2013.

Elsworth, G., Lovenduski, N., McKinnon, K., Krumhardt, K., and Brady, R.: Finding the Fingerprint of Anthropogenic Climate Change in Marine Phytoplankton Abundance, Current Climate Change Reports, 6, doi:10.1007/s40641-020-00156-w, 2020.

Elsworth, G., Lovenduski, N., and McKinnon, K.: Alternate History: A Synthetic Ensemble of Ocean Chlorophyll Concentrations, Global Biogeochemical Cycles, 35, 2021.

Falkowski, P.: Ocean Science: The power of plankton, Nature, 483, S17–20, doi:10.1038/483S17a, 2012.

FAO: The State of World Fisheries and Aquaculture 2020. Sustainability in action., Rome., doi:10.4060/ca9229en, 2020.

Flanagan, P., Jensen, O., Morley, J., and Pinsky, M.: Response of marine communities to local temperature changes, Ecography, 42, doi:10.1111/ecog.03961, 2018.

Geider, R., Macintyre, H., and Kana, T.: A dynamic regulatory model of phytoplanktonic acclimation to light, nutrients, and temperature, Limnology and Oceanography, 43, 679–694, doi:10.4319/lo.1998.43.4.0679, 1998.

Giorgetta, M., Jungclaus, J., Reick, C., Legutke, S., Bader, J., Böttinger, M., Brovkin, V., Crueger, T., Esch, M., Fieg, K., Gorges, K., Gayler, V., Haak, H., Hollweg, H.-D., Ilyina, T., Kinne, S., Kornblueh, L., Matei, D., Mauritsen, T., and Stevens, B.: Climate and carbon cycle changes from 1850 to 2100 in MPI-ESM simulations for the Coupled Model Intercomparison Project Phase 5, Journal of Advances in Modeling Earth Systems, 5, doi:10.1002/jame.20038, 2013.

Hashioka, T., Vogt, M., Yamanaka, Y., Le Quéré, C., Buitenhuis, E., Aita, M., Alvain, S., Bopp, L., Hirata, T., Lima, I., Sailley, S., and Doney, S.: Phytoplankton competition during the spring bloom in four Plankton Functional Type Models, Biogeosciences Discussions, 9, doi:10.5194/bgd-9-18083-2012, 2012.

Heneghan, R., Galbraith, E., Blanchard, J., Harrison, C., Barrier, N., Bulman, C., Cheung, W., Coll, M., Eddy, T., Erauskin-Extramiana, M., Everett, J., Fernandes, J., Guiet, J., Maury, O., Palacios Abrantes, J., Petrik, C., Du Pontavice, H., Richardson, A., and Tittensor, D.: Disentangling diverse responses to climate change among global marine ecosystem models, Progress in Oceanography, 198, 102 659, doi:10.1016/j.pocean.2021.102659, 2021.

Hurrell, J. W., Holland, M. M., Gent, P. R., Ghan, S., Kay, J. E., Kushner, P. J., Lamarque, J.-F., Large, W. G., Lawrence, D., Lindsay, K., Lipscomb, W. H., Long, M. C., Mahowald, N., Marsh, D. R., Neale, R. B., Rasch, P., Vavrus, S., Vertenstein, M., Bader, D., Collins, W. D., Hack, J. J., Kiehl, J., and Marshall, S.: The Community Earth System Model: A framework for collaborative research, Bulletin of the American Meteorological Society, 94, 1339–1360, doi:10.1175/BAMS-D-12-00121.1, 2013.

Ilyina, T., Six, K., Segschneider, J., Maier-Reimer, E., Li, H., and Núñez-Riboni, I.: Global ocean biogeochemistry model HAMOCC: Model architecture and performance as component of the MPI-Earth System Model in different CMIP5 experimental realizations, Journal of Advances in Modeling Earth Systems, 5, doi:10.1029/2012MS000178, 2013.

Jennings, S. and Collingridge, K.: Predicting Consumer Biomass, Size-Structure, Production, Catch Potential, Responses to Fishing and Associated Uncertainties in the World's Marine Ecosystems, PLoS ONE, 10, doi:10.1371/journal.pone.0133794, 2015.

Kay, J. E., Deser, C., Phillips, A., Mai, A., Hannay, C., Strand, G., Arblaster, J. M., Bates, S. C., Danabasoglu, G., Edwards, J., Holland, M., Kushner, P., Lamarque, J.-F., Lawrence, D., Lindsay, K., Middleton, A., Munoz, E., Neale, R., Oleson, K., Polvani, L., and Vertenstein, M.: The Community Earth System Model (CESM) Large Ensemble project: A community resource for studying climate change in the presence of internal climate variability, Bulletin of the American Meteorological Society, 96, 1333–1349, doi:10.1175/BAMS-D-13-00255.1, 2015.

Kostadinov, T., Milutinovic, S., Marinov, I., and Cabre, A.: Carbon-based phytoplankton size classes retrieved via ocean color estimates of the particle size distribution, Ocean Science (OS), 12, 561–575, doi:10.5194/os-12-561-2016, 2016.

Krumhardt, K., Lovenduski, N., Long, M., Levy, M., Lindsay, K., Moore, J., and Nissen, C.: Coccolithophore Growth and Calcification in an Acidified Ocean: Insights From Community Earth System Model Simulations, Journal of Advances in Modeling Earth Systems, 11, doi:10.1029/2018MS001483, 2019.

Kwiatkowski, L. and Orr, J.: Diverging seasonal extremes for ocean acidification during the twenty-first century, Nature Climate Change, 8, 141–146, doi:10.1038/s41558-017-0054-0, 2018.

Kwiatkowski, L., Torres, O., Bopp, L., Aumont, O., Chamberlain, M., Christian, J., Dunne, J., Gehlen, M., Ilyina, T., John, J., Lenton, A., Li, H., Lovenduski, N., Orr, J., Palmiéri, J., Santana-Falcón, Y., Schwinger, J., Séférian, R., Stock, C., and Ziehn, T.: Twenty-first century ocean warming, acidification, deoxygenation, and upper-ocean nutrient and primary production decline from CMIP6 model projections, Biogeosciences, 17, 3439–3470, doi:10.5194/bg-17-3439-2020, 2020.

Lamarque, J., Bond, T., Eyring, V., Granier, C., Heil, A., Klimont, Z., Lee, D., Liousse, C., Mieville, A., Owen, B., Schultz, M., Shindell, D., Smith, S., Stehfest, E., Aardenne, J., Cooper, O., Kainuma, M., Mahowald, N., Mcconnell, J., and Vuuren, D.: Historical (1850-2000) gridded anthropogenic and biomass burning emissions of reactive gases and aerosols: methodology and application, Atmospheric Chemistry and Physics, 10, 7017–7039, doi:10.5194/acpd-10-4963-2010, 2010.

Landschützer, P., Gruber, N., Bakker, D., Stemmler, I., and Six, K.: Strengthening seasonal marine CO_2 variations due to increasing atmospheric CO_2, Nature Climate Change, 8, 146–150, doi:10.1038/s41558-017-0057-x, 2018.

Laufkötter, C., Vogt, M., Gruber, N., Aita-Noguchi, M., Aumont, O., Bopp, L., Buitenhuis, E., Doney, S., Dunne, J., Hashioka, T., Hauck, J., Hirata, T., John, J., Le Quéré, C., Lima, I., Nakano, H., Séférian, R., Totterdell, I., Vichi, M., and Voelker, C.: Drivers and uncertainties of future global marine primary production in marine ecosystem models, Biogeosciences Discussions, 12, 3731–3824, doi:10.5194/bgd-12-3731-2015, 2015.

Lehodey, P., Murtugudde, R., and Senina, I.: Bridging the gap from ocean models to population dynamics of large marine predators: A model of mid-trophic functional groups, Progress In Oceanography, 84, 69–84, doi:10.1016/j.pocean.2009.09.008, 2010.

Link, J. and Marshak, A.: Characterizing and comparing marine fisheries ecosystems in the United States: determinants of success in moving toward ecosystem-based fisheries management, Reviews in Fish Biology and Fisheries, 29, doi:10.1007/s11160-018-9544-z, 2019.

Long, M., Moore, J., Lindsay, K., Levy, M., Doney, S., Luo, J., Krumhardt, K., Letscher, R., Grover, M., and Sylvester, Z.: Simulations with the Marine Biogeochemistry Library (MARBL), Journal of Advances in Modeling Earth Systems, doi:10.1002/essoar.10507358.1, 2021.

Longhurst, A.: Ecological Geography of the Sea, Academic Press, doi:10.1016/B978-012455521-1/50002-4, 2007.

Lotze, H., Tittensor, D., Bryndum-Buchholz, A., Eddy, T., Cheung, W., Galbraith, E., Barange, M., Barrier, N., Bianchi, D., Blanchard, J., Bopp, L., Büchner, M., Bulman, C., Carozza, D., Christensen, V., Coll, M., Dunne, J., Fulton, E., Jennings, S., and Worm, B.: Global ensemble projections reveal trophic amplification of ocean biomass declines with climate change, Proceedings of the National Academy of Sciences, 10, doi:10.1073/pnas.1900194116, 2019.

Manabe, S. and Ronald, S.: Century-Scale Effects of Increased Atmospheric CO2 on the Ocean-Atmosphere System, Nature, 364, 215–218, doi:10.1038/364215a0, 1993.

Marshak, A. and Link, J.: Primary production ultimately limits fisheries economic performance, Scientific Reports, 11, 12 154, doi:10.1038/s41598-021-91599-0, 2021.

Martinez-Vicente, V., Evers-King, H., Roy, S., Kostadinov, T., Tarran, G., Graff, J., Brewin, B., Dall'Olmo, G., Jackson, T., Hickman, A., Röttgers, R., Krasemann, H., Maranon, E., Platt, T., and Sathyendranath, S.: Intercomparison of Ocean Color Algorithms for Picophytoplankton Carbon in the Ocean, Frontiers in Marine Science, 4, doi:10.3389/fmars.2017.00378, 2017.

Maury, O.: An overview of APECOSM, a spatialized mass balanced "Apex Predators ECOSystem Model" to study physiologically structured tuna population dynamics in their ecosystem, Progress In Oceanography, 84, 113–117, doi:10.1016/j.pocean.2009.09.013, 2010.

McKinnon, K. and Deser, C.: Internal variability and regional climate trends in an observational large ensemble, Journal of Climate, 31, 6783–6802, doi:10.1175/JCLI-D-17-0901.1, 2018.

McKinnon, K., Poppick, A., Dunn-Sigouin, E., and Deser, C.: An "observational large ensemble" to compare observed and modeled temperature trend uncertainty due to internal variability, Journal of Climate, 30, 7585–7598, doi:10.1175/JCLI-D-16-0905.1, 2017.

Meehl, G., Goddard, L., Murphy, J., Ronald, S., Boer, G., Danabasoglu, G., Dixon, K., Giorgetta, M., Greene, A., Hawkins, E., Hegerl, G., Karoly, D., Keenlyside, N., Kimoto, M., Kirtman, B., Navarra, A., Pulwarty, R., Smith, D., Stammer, D., and Stockdale, T.: Decadal Prediction. Can It Be Skillful?, Bulletin of the American Meteorological Society, 2009.

Meehl, G., Hu, A., Arblaster, J., Fasullo, J., and Trenberth, K.: Externally Forced and Internally Generated Decadal Climate Variability Associated with the Interdecadal Pacific Oscillation, Journal of Climate, 26, 7298–7310, doi:10.1175/JCLI-D-12-00548.1, 2013.

Meehl, G., Goddard, L., Boer, G., Burgman, R., Branstator, G., Cassou, C., Corti, S., Danabasoglu, G., Doblas-Reyes, F., Hawkins, E., Karspeck, A., Kimoto, M., Kumar, A., Matei, D., Mignot, J., Msadek, R., Pohlmann, H., Rienecker, M., Rosati, T., and Yeager, S.: Decadal Climate Prediction: An Update from the Trenches, Bulletin of the American Meteorological Society, 95, 243–267, doi:10.1175/BAMS-D-12-00241.1, 2014.

Meinshausen, M., Smith, S., Calvin, K., Daniel, J., Kainuma, M., Lamarque, J.-F., Matsumoto, K., Montzka, S., Raper, S., Riahi, K., Thomson, A., Velders, G. J. M., and Vuuren, D.: The RCP greenhouse gas concentrations and their extensions from 1765 to 2300, Climatic Change, 109, 213–241, doi:10.1007/s10584-011-0156-z, 2011.

Mills, K., Pershing, A., Brown, C., Chen, Y., Chiang, F.-S., Holland, D., Lehuta, S., Nye, J., Sun, J., Thomas, A., and Wahle, R.: Fisheries Management in a Changing Climate: Lessons From the 2012 Ocean Heat Wave in the Northwest Atlantic, Oceanography, 26, doi:10.5670/oceanog.2013.27, 2013.

Moore, C., Morley, J., Morrison, B., Kolian, M., Horsch, E., Frolicher, T., Pinsky, M., and Griffis, R.: Estimating the Economic Impacts of Climate Change on 16 Major U.S. Fisheries, Climate Change Economics, doi:10.1142/S2010007821500020, 2021.

Moore, J. and Braucher, O.: Sedimentary and mineral dust sources of dissolved iron to the world ocean, Biogeosciences, 5, doi:10.5194/bgd-4-1279-2007, 2008.

Moore, J., Lindsay, K., Doney, S., Long, M., and Misumi, K.: Marine Ecosystem Dynamics and Biogeochemical Cycling in the Community Earth System Model [CESM1(BGC)]: Comparison of the 1990s with the 2090s under the RCP4.5 and RCP8.5 Scenarios, Journal of Climate, 26, 9291–9312, doi:10.1175/JCLI-D-12-00566.1, 2013.

Moore, K., Doney, S., and Lindsay, K.: Upper ocean ecosystem dynamics and iron cycling in a global three-dimensional model, Global Biogeochemical Cycles, 18, doi:10.1029/2004GB002220, 2004.

Pauly, D. and Christensen, V.: Pauly, D. and Christensen, V. Primary production required to sustain global fisheries. Nature 374, 255-257, Nature, 374, doi:10.1038/374255a0, 1995.

Perry, A., Low, P., Ellis, J., and Reynolds, J.: Climate Change and Distribution Shifts in Marine Fishes, Science, 308, 1912–1915, doi:10.1126/science.1111322, 2005.

Petrik, C., Stock, C., Andersen, K., van Denderen, D., and Watson, J.: Bottom-up drivers of global patterns of demersal, forage, and pelagic fishes, Progress in Oceanography, 176, 102 124, doi:10.1016/j.pocean.2019.102124, 2019.

Prowe, A. F., Pahlow, M., Dutkiewicz, S., Follows, M., and Oschlies, A.: Top-down control of marine phytoplankton diversity in a global ecosystem model, Progress In Oceanography, 101, doi:10.1016/j.pocean.2011.11.016, 2012a.

Prowe, A. F., Pahlow, M., and Oschlies, A.: Controls on the diversity–productivity relationship in a marine ecosystem model, Ecological Modelling, 225, 167–176, doi:10.1016/j.ecolmodel.2011.11.018, 2012b.

Resplandy, L., Séférian, R., and Bopp, L.: Natural variability of CO_2 and O_2 fluxes: What can we learn from centuries-long climate models simulations?, Journal of Geophysical Research: Oceans, 120, 384–404, doi:10.1002/2014JC010463, 2015.

Rodgers, K., Lee, S.-S., Rosenbloom, N., Timmermann, A., Danabasoglu, G., Deser, C., Edwards, J., Kim, J.-E., Simpson, I., Stein, K., Stuecker, M., Yamaguchi, R., Bódai, T., Chung, E.-S., Huang, L., Kim, W., Lamarque, J.-F., Lombardozzi, D., Wieder, W., and Yeager, S.: Ubiquity of human-induced changes in climate variability, Earth System Dynamics, doi:10.5194/esd-2021-50, 2021.

Roy, S., Sathyendranath, S., and Platt, T.: Size-partitioned phytoplankton carbon and carbon-to-chlorophyll ratio from ocean colour by an absorption-based bio-optical algorithm, Remote Sensing of Environment, 194, 177–189, doi:10.1016/j.rse.2017.02.015, 2017.

Santer, B., Mears, C., Doutriaux, C., Caldwell, P., Gleckler, P., Wigley, T., Solomon, S., Gillett, N., Ivanova, D., Karl, T., Lanzante, J., Meehl, G., Stott, P., Taylor, K., Thorne, P., Wehner, M., and Wentz, F.: Separating signal and noise in atmospheric temperature changes: The importance of timescale, Journal of Geophysical Research (Atmospheres), 116, doi:10.1029/2011JD016263, 2011.

Sathyendranath, S., Platt, T., Kovac, Z., Dingle, J., Jackson, T., Brewin, B., Franks, P., Maranon, E., Kulk, G., and Bouman, H.: Reconciling models of primary production and photoacclimation, Applied Optics, 59, doi:10.1364/AO.386252, 2020.

Schmittner, A.: Decline of the marine ecosystem caused by a reduction in the Atlantic overturning circulation, Nature, 434, 628–33, doi:10.1038/nature03476, 2005.

Schneider, D. and Deser, C.: Tropically driven and externally forced patterns of Antarctic sea ice change: reconciling observed and modeled trends, Climate Dynamics, 50, doi:10.1007/s00382-017-3893-5, 2018.

Staudinger, M., Mills, K., Stamieszkin, K., Record, N., Hudak, C., Allyn, A., Diamond, T., Friedland, K., Golet, W., Henderson, M., Hernandez, C., Huntington, T., Ji, R., Johnson, C., Johnson, D., Jordaan, A., Kocik, J., Li, Y., Liebman, M., and Yakola, K.: It's about time: A synthesis of changing phenology in the Gulf of Maine ecosystem, Fisheries Oceanography, 28, doi:10.1111/fog.12429, 2019.

Steinacher, M., Joos, F., Frölicher, T., Bopp, L., Cadule, P., Cocco, V., Doney, S., Gehlen, M., Lindsay, K., Moore, J., Schneider, B., and Segschneider, J.: Projected 21st century decrease in marine productivity: A multi-model analysis, Biogeosciences, 7, 979–1005, doi:10.5194/bg-7-979-2010, 2010.

Stock, C., John, J., Rykaczewski, R., Asch, R., Cheung, W., Dunne, J., Friedland, K., Lam, V., Sarmiento, J., and Watson, R.: Reconciling fisheries catch and ocean productivity, Proceedings of the National Academy of Sciences, 114, doi:10.1073/pnas.1610238114, 2017.

Stocker, T. and Schmittner, A.: Influence of CO2 emission rates on the stability of the thermohaline circulation, Nature, 388, 862–865, doi:10.1038/42224, 1997.

Tagliabue, A., Kwiatkowski, L., Bopp, L., Butenschön, M., Cheung, W., Lengaigne, M., and Vialard, J.: Persistent Uncertainties in Ocean Net Primary Production Climate Change Projections at Regional Scales Raise Challenges for Assessing Impacts on Ecosystem Services, Frontiers in Climate, 3, 738 224, doi:10.3389/fclim.2021.738224, 2021.

Taylor, K., Ronald, S., and Meehl, G.: An overview of CMIP5 and the Experiment Design, Bulletin of the American Meteorological Society, 93, 485–498, doi:10.1175/BAMS-D-11-00094.1, 2011.

Timmermann, A., Oberhuber, J., Bacher, A., Esch, M., Latif, M., and Roeckner, E.: Increased El Niño frequency in a climate model forced by future greenhouse warming, Nature, 398, 694–697, doi:10.1038/19505, 1999.

Tittensor, D., Eddy, T., Lotze, H., Galbraith, E., Cheung, W., Barange, M., Blanchard, J., Bopp, L., Bryndum-Buchholz, A., Büchner, M., Bulman, C., Carozza, D., Christensen, V., Coll, M., Dunne, J., Fernandes, J., Fulton, E., Hobday, A., Huber, V., and Walker, N.: A protocol for the intercomparison of marine fishery and ecosystem models: Fish-MIP v1.0, Geoscientific Model Development, 11, 1421–1442, doi:10.5194/gmd-11-1421-2018, 2018.

Tittensor, D., Blanchard, J., Fulton, E., Cheung, W., Novaglio, C., Harrison, C., Heneghan, R., Barrier, N., Bianchi, D., Bopp, L., Bryndum-Buchholz, A., Britten, G., Büchner, M., Christensen, V., Coll, M., Dunne, J., Eddy, T., Everett, J., Fernandes, J., and Stock, C.: Next-generation ensemble projections reveal higher climate risks for marine ecosystems, Nature Climate Change, doi:10.1038/s41558-021-01173-9, 2021.

Travers-Trolet, M., Shin, Y.-J., Jennings, S., Machu, E., Huggett, J., Field, J., and Cury, P.: Two-way coupling versus one-way forcing of plankton and fish models to predict ecosystem changes in the Benguela, Ecological Modelling, 220, 3089–3099, doi:10.1016/j.ecolmodel.2009.08.016, 2009.

Vichi, M., Allen, I., Masina, S., and Hardman-Mountford, N.: The emergence of ocean biogeochemical provinces: A quantitative assessment and a diagnostic for model evaluation, Global Biogeochemical Cycles, 25, doi:10.1029/2010GB003867, 2011.

Wernberg, T., Bennett, S., Babcock, R., de Bettignies, T., Cure, K., Depczynski, M., Dufois, F., Fromont, J., Fulton, C., Hovey, R., Harvey, E., Holmes, T., Kendrick, G., Radford, B., Santana-Garcon, J., Saunders, B., Smale, D., Thomsen, M., Tuckett, C., and Wilson, S.: Climate-driven regime shift of a temperate marine ecosystem, Science, 353, 169–172, doi:10.1126/science.aad8745, 2016.

Yamaguchi, R., Rodgers, K., Timmermann, A., Stein, K., Schlunegger, S., Bianchi, D., Dunne, J., and Slater, R.: Trophic level decoupling drives future changes in phytoplankton bloom phenology, Nature Climate Change, 12, 1–8, doi:10.1038/s41558-022-01353-1, 2022.

Supplemental information

In our discussion of zooplankton grazing as a ~~driver of~~ contributor to changing phytoplankton variance with anthropogenic warming, we consider the parameterization of zooplankton grazing in the CESM1-LE. The biogeochemical ecosystem model simulates a single generic zooplankton functional type (ZFT) with different grazing rates and half saturation constants prescribed for different PFTs (e.g. slower zooplankton grazing rates for larger phytoplankton). Grazing rate for the single ZFT is computed using a Holling Type III (sigmoidal) relationship:

$$G = g_{max} \cdot T_{lim} \cdot Z \cdot \frac{P^2}{P^2 + K^2} \tag{5}$$

where g_{max} is the maximum grazing rate, T_{lim} is the temperature limitation (Q10) function, Z is the zooplankton concentration, P is the phytoplankton concentration, and K is the half-saturation constant for grazing. Zooplankton loss scales with temperature and a linear mortality term which represents zooplankton losses from predation.

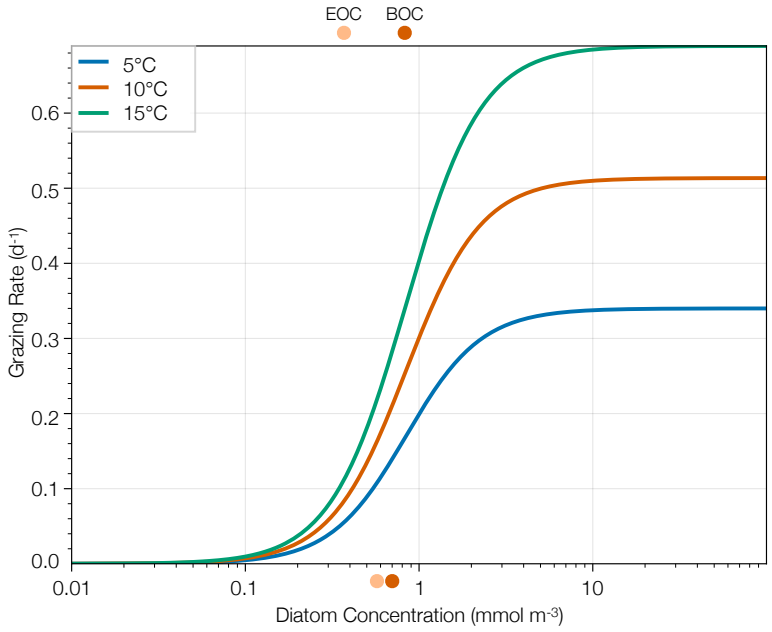

Figure S1. Holling Type III (sigmoidal) functional parameterization of zooplankton grazing rate in the biogeochemical ecosystem model of the CESM1-LE across a range of temperatures. Changes in diatom concentration between the beginning and end of the century (BOC and EOC, respectively) are shown in the dark and light orange circles, respectively, with the changes in the ASP region shown above and changes in the SAP region shown below.

Figure S1 illustrates changes in grazing rate as a function of diatom concentration using this parameterization. To approximate the effects of climatic warming, we plot the relationship for across a series of increasing temperatures: (blue) 5°C, (orange) 10°C, and (green) 15°C. The maximum grazing rate increases with warming temperatures. Changes in diatom concentration in mmol m^{-3} between the beginning and end of the century are denoted by dark and light orange circles, respectively.

To provide context for the CESM1-LE results, we examine changes in chlorophyll variance from a subset of the Coupled Model Intercomparison Project 5 (CMIP5) models (Taylor et al., 2011): the GFDL-ESM2M from the Geophysical Fluid Dynamics Laboratory (GFDL; (Dunne et al., 2012, 2013), the CanESM2 from the Canadian Centre for Climate Modelling and Analysis (Christian et al., 2010; Arora et al., 2011), and the MPI-ESM-LR from the Max Planck Institute (MPI; (Giorgetta et al., 2013; Ilyina et al., 2013), consisting of 30, 50, and 100 ensemble members, respectively. Similarly to the CESM1-LE, historical forcing was applied through 2005, followed by RCP8.5 forcing through 2100.

We compare the variance in chlorophyll observed among the large ensembles to a synthetic ensemble generated from observational chlorophyll concentrations over the MODIS remote sensing record (Elsworth et al., 2020, 2021). A synthetic ensemble is a ~~novel~~ technique that allows the observational record to be statistically emulated to create multiple possible evolutions of the observed record, each with a unique sampling of internal climate variability (McKinnon et al., 2017; McKinnon and Deser, 2018). We use the synthetic ensemble of chlorophyll concentration to compare the variability observed in the real world to the variability simulated across a suite of ESM ensembles.

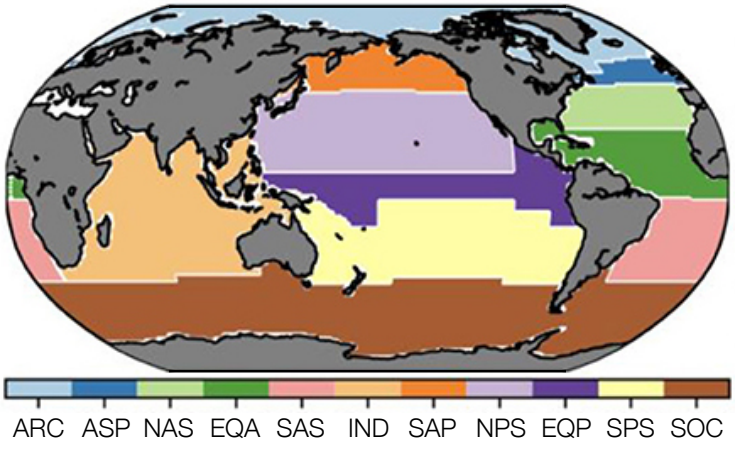

Figure S2. ~~Holling Type III (sigmoidal) functional parameterization of zooplankton grazing rate~~ The 11 ocean ecological provinces defined in ~~the biogeochemical ecosystem model of the CESM1-LE across a range of temperatures. Changes in diatom concentration between the beginning~~ Tagliabue et al. (2021) and ~~end~~ Vichi et al. (2011). Provinces were aggregated using multivariate statistical analysis of ~~the century~~ physical (~~BOC and EOC~~i.e., ~~respectively~~salinity, temperature, mixed layer depth) ~~are shown in the dark~~ and ~~light orange circles~~biological (i.e., ~~respectively,~~ chlorophyll concentration) ocean parameters to group ocean regions with ~~the changes in the ASP region shown above~~ similar physical and ~~changes in the SAP region shown below~~environmental conditions. Figure adapted from Tagliabue et al. (2021).

Table S1. The temporal standard deviation of phytoplankton biomass ($\sigma_{temporal}$) for ensemble member 1 of the CESM1-LE and the satellite observations from 1998 to 2019 averaged across the 11 ecological provinces defined in Vichi et al. (2011) and Tagliabue et al. (2021). Units are mg C m^{-3}.

Biome	Name	$\sigma_{temporal,model}$	$\sigma_{temporal,obs}$
ARC	Arctic	2.7	4.5
ASP	Atlantic subpolar	9.7	4.1
NAS	North Atlantic subtropical gyre	2.8	1.7
EQA	Equatorial Atlantic	1.3	1.4
SAS	South Atlantic subtropical gyre	1.1	1.2
IND	Indian Ocean	0.81	2.0
SAP	subarctic Pacific	3.7	4.0
NPS	North Pacific subtropical gyre	0.85	1.5
EQP	Equatorial Pacific	5.8	1.8
SPS	South Pacific subtropical gyre	0.60	0.93
SOC	Southern Ocean	2.7	2.7

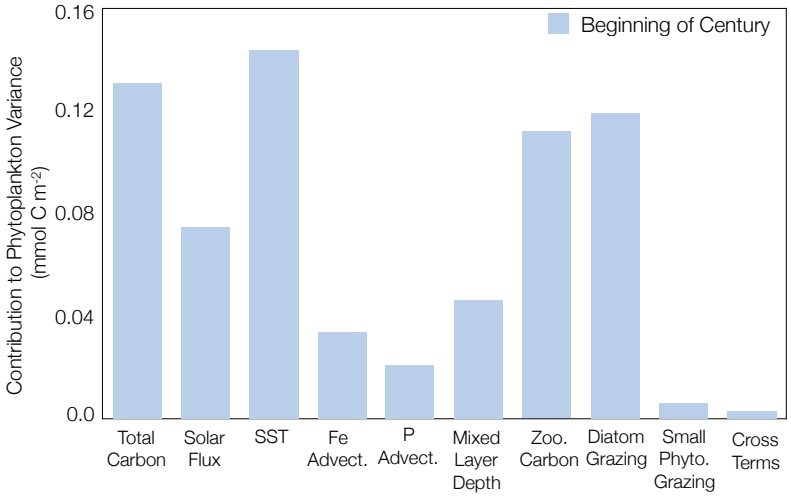

Figure S3. Reconstructed contributions of each variable to phytoplankton biomass variance at the beginning of the RCP8.5 forcing scenario (2006 to 2016). The contribution of cross terms to the MLR reconstruction is shown in the rightmost bar. The variance is calculated using the average across the first (2006 to 2016) decade of the RCP8.5 forcing scenario.

To provide context for Figure 3, we include the spatial distribution of total phytoplankton carbon concentration (Figure ~~S4~~S5a) and internal standard deviation in phytoplankton carbon concentration (Figure ~~S4~~S5b) simulated by the CESM1-LE across the RCP8.5 forcing scenario (2006 to 2100). Total phytoplankton carbon concentration is relatively high in the subpolar Atlantic and Pacific, the Southern

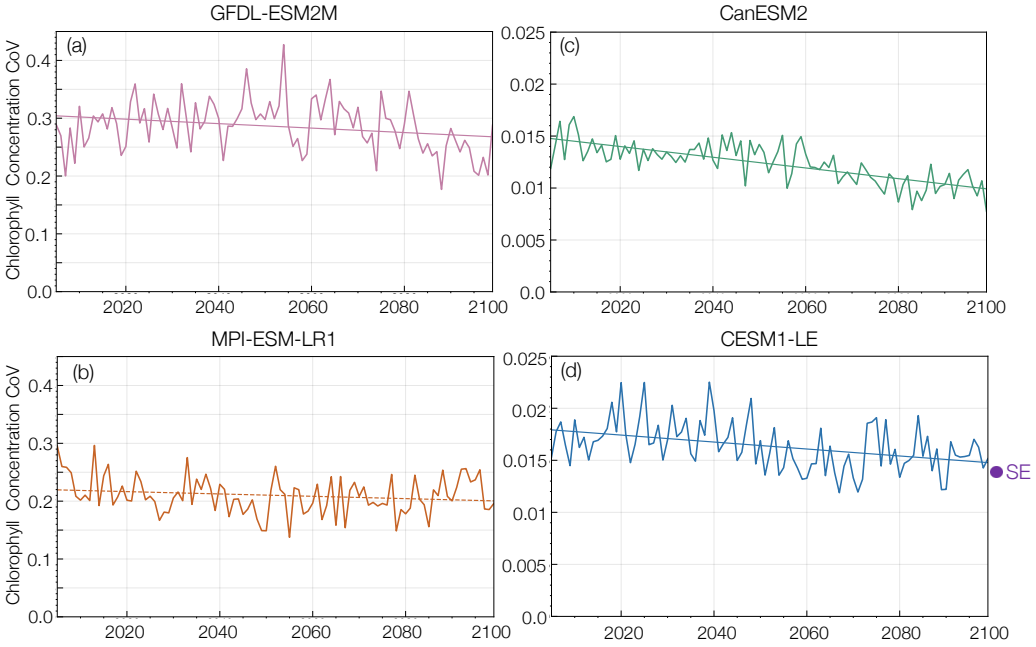

Figure S4. Coefficient of variance (internal standard deviation divided by ensemble mean) in annual mean global surface ocean chlorophyll concentration from 2006 to 2100 across a suite of CMIP5 model ensembles: (a) (pink) GFDL-ESM2M (b) (orange) MPI-ESM-LR1 (c) (green) CanESM2 (d) (blue) CESM1-LE. The average coefficient of variance of the synthetic ensemble (SE) created using the MODIS surface ocean chlorophyll record is shown in the purple dot on the vertical axis (Elsworth et al., 2020, 2021). Trend significance is determined by a t-test with a p-value less than 0.05.

Ocean, and the Eastern Equatorial Upwelling Zone and relatively low in the subtropical gyre regions (Figure ~~S4~~S5a). Regions of relatively high phytoplankton carbon concentrations correspond to regions of high variance (Figure ~~S4~~S5b).

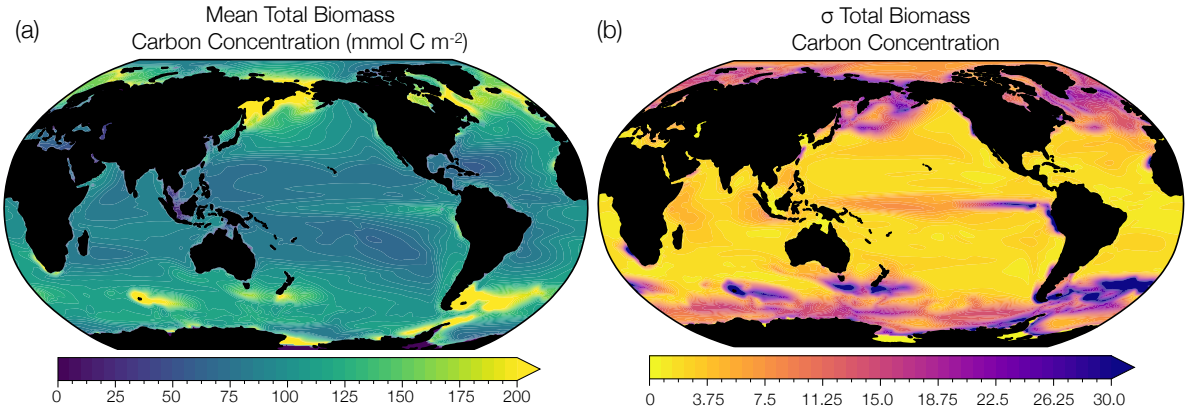

~~(a) Total phytoplankton carbon concentration simulated by the CESM1-LE in mmol C m^{-2} averaged across the RCP8.5 forcing scenario (2006 to 2100). (b) Internal standard deviation in total phytoplankton carbon concentration averaged over the same period.~~

Figure S5. (a) Total phytoplankton carbon concentration simulated by the CESM1-LE in mmol C m^{-2} averaged across the RCP8.5 forcing scenario (2006 to 2100). (b) Internal standard deviation in total phytoplankton carbon concentration averaged over the same period. The change in the coefficient of variance is calculated using averages across the first (2006 to 2016) and last (2090 to 2100) decades of the RCP8.5 forcing scenario.

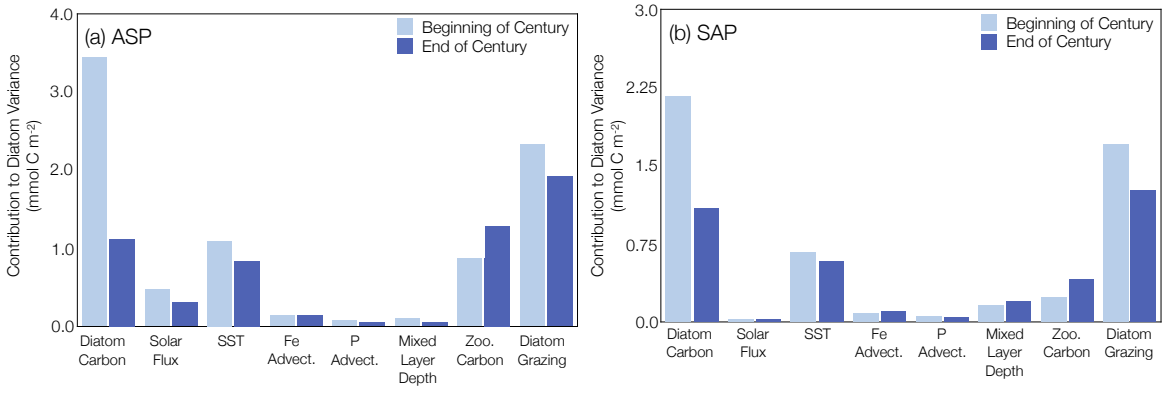

Figure S6. Reconstructed changes in the contribution of each ~~driver~~ variable to phytoplankton biomass variance across the RCP8.5 forcing scenario (2006 to 2100) using variable regression coefficients between the beginning and end of the century. Regions were selected which aligned with the highest fisheries catch in the (a) Atlantic and (b) Pacific basins with the beginning of the century shown in light blue and the end of the century shown in dark blue. The change in the coefficient of variance is calculated using averages across the first (2006 to 2016) and last (2090 to 2100) decades of the RCP8.5 forcing scenario.

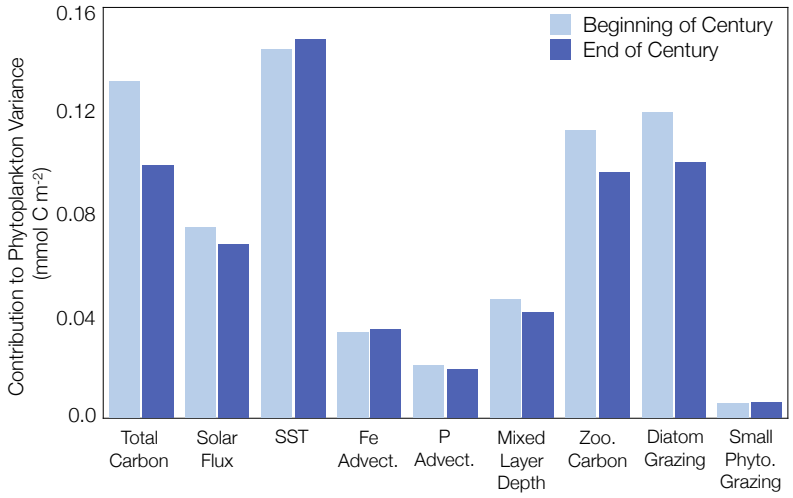

Figure S7. Reconstructed global changes in the contribution of each ~~driver~~ variable to changes in ~~(a) mean~~ phytoplankton biomass ~~and (b) phytoplankton biomass~~ variance across the RCP8.5 forcing scenario (2006 to 2100). The beginning of the century is shown in light blue and the end of the century is shown in dark blue.

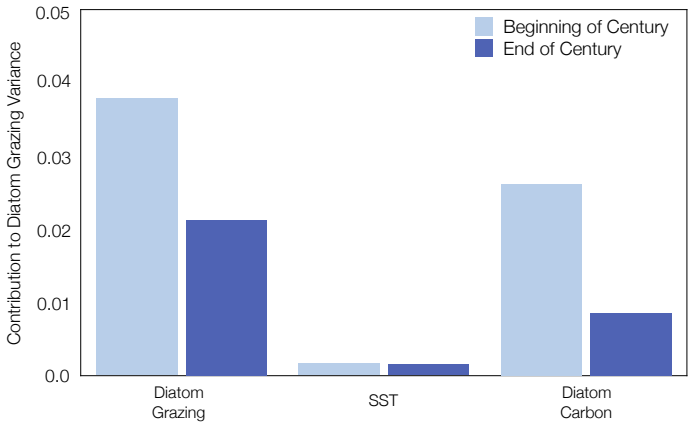

Figure S8. Reconstructed changes in the contribution of ~~each driver variable~~ sea surface temperature and diatom carbon to ~~mean phytoplankton biomass~~ changes in diatom grazing variance in the Atlantic supolar (ASP) region across the RCP8.5 forcing scenario (2006 to 2100)~~with the beginning~~ . The contribution of the ~~century shown~~ change in ~~light blue and~~ diatom biomass variance dominates the ~~end of the century shown~~ change in ~~dark blue~~diatom grazing variance. ~~Marine ecological regions are defined~~ The change in ~~Tagliabue et al. (2021) . Regions were selected which aligned with~~ variance is calculated using averages across the ~~highest fisheries catch in the~~ first (a2006 to 2016) ~~Atlantic~~ and last (b2090 to 2100) ~~Pacific basins and~~ decades of the ~~biogeochemically important (c) Southern Ocean and (d) Equatorial Pacific regions~~RCP8.5 forcing scenario.~~The dominant phytoplankton functional type is considered in each region. In regions with a mixed ecological assemblage, total phytoplankton carbon is considered.~~

~~Reconstructed changes in the contribution of sea surface temperature and diatom carbon to changes in diatom grazing variance in the Atlantic supolar (ASP) region across the RCP8.5 forcing scenario (2006 to 2100). The contribution of the change in diatom biomass variance dominates the change in diatom grazing variance.~~